npj | microgravity

Article

Published in cooperation with the Biodesign Institute at Arizona State University, with the support of NASA

https://doi.org/10.1038/s41526-025-00507-7

25-hydroxysterol mitigates microgravity-induced retinal damage by suppressing microglial inflammation through disrupting lipid raft formation

Jee Hoon Lee[1] & Dae Yu Kim[1,2,3] ✉

Spaceflight-associated neuro-ocular syndrome (SANS) poses a significant risk to astronaut vision during long-duration missions, yet its immunological underpinnings remain poorly defined. Here, we identify retinal microglia as key mediators of ocular degeneration under simulated microgravity (SMG). Using a 3D clinostat model, we show that SMG induces early activation of retinal pigment epithelium (RPE), which in turn promotes microglial activation and triggers a feedforward cascade of RPE damage and neuronal loss. We further demonstrate that 25-hydroxycholesterol (25-HC), an oxysterol capable of penetrating the blood-retinal barrier, attenuates this inflammatory cascade by disrupting lipid raft formation in microglia. Low-dose 25-HC suppresses the recruitment of cytokine receptors to lipid rafts, mitigating microglia-driven retinal injury. These findings uncover a critical immunopathological axis underlying SANS and propose 25-HC as a non-invasive, immunomodulatory countermeasure to preserve retinal integrity during spaceflight.

With humanity entering a new space age, extended human spaceflight is almost a tangible reality. Therefore, understanding the effects of long-term space travel on the human body is now critical. Among the many extreme conditions encounterable during space exploration, microgravity (μG) is a major factor that affects normal bodily function through the redistribution of fluid throughout the body. Specifically, astronauts can suffer from vision problems during spaceflight, which has been referred to as "spaceflight-associated neuro-ocular syndrome" (SANS). Post-flight data from approximately 300 astronauts revealed that 23% of astronauts on short-duration missions and 48% of astronauts on long-duration missions experienced near-vision difficulties, including ocular issues such as optic disc edema, globe flattening, choroidal folds, and refractive error shifts[1,2]. Although the characteristic symptoms of SANS are known, the factors and mechanisms associated with SANS are yet to be understood.

Although the underlying pathogenesis of SANS remains unclear and its etiology is multifactorial, several hypotheses have been proposed, based on factors including elevated intracranial pressure (ICP), the ocular glymphatic system, upward brain shift, and secondary changes in tissue[3,4]. Recently, some studies have suggested that ocular inflammation and immune alterations may also be associated with SANS. An elevated ICP that is relieved upon return to a 1G environment may induce secondary inflammation or oxidative stress[4]. Crucian et al. reported increased levels of inflammatory cytokine profiles in astronauts with SANS[5]. Zanello et al. observed that the expression of oxidative and cellular-response genes was increased in retina samples from mice subjected to shuttle missions[6]. These results suggest that dysregulation of the ocular immune system under spaceflight conditions may contribute to the pathology of SANS. Since the interplay between ocular immunology and space μG–induced SANS remains ill-defined, the underlying mechanism through which the ocular immune system contributes to SANS must be investigated.

Microglia are the main resident immune cells of the central nervous system (CNS), including the retina. In their homeostatic state, microglia are located in the inner and outer plexiform layers, as well as in the ganglion cell layer, where they perform multiple functions, such as regulating innate and adaptive immune responses, neurotrophic support, and synaptic refinement[7–9]. However, various harmful insults can trigger a reactive phenotype of microglia via increased inflammatory mediator secretion, morphological changes, and migration to the injury site, leading to retinal damage and neuronal death[9–12]. Recently, some studies have suggested that microglia can be activated by μG exposure, leading to CNS damage. In

[1]Inha Research Institute for Aerospace Medicine, Inha University, Incheon, 22212, Republic of Korea. [2]Department of Electrical and Computer Engineering, College of Engineering, Inha University, Incheon, 22212, Republic of Korea. [3]Center for Sensor Systems, Inha University, Incheon, 22212, Republic of Korea.
✉e-mail: dyukim@inha.ac.kr

studies conducted using a hindlimb uploading rodent model, the activation and inflammatory response of microglia were detected in the brain[13,14]. In the BV-2 microglial cell line, microglial activation was also observed under 2D clinorotation-induced μG[15]. Although microglial activation may be involved in μG-induced retinal damage, most studies have focused on the brain rather than the eye. Given the important role of ocular immune response in the pathology of retinal damage, determining whether microglial activation is involved in retinal damage under μG conditions is important to ensure that effective strategies for suppressing microglial activation can be formulated accordingly.

Recent studies have suggested that multiple inflammatory signaling events in microglia are organized in lipid rafts, which are distinct structures in the plasma membrane[16,17]. Lipid rafts are cholesterol-enriched plasma membrane microdomains that orchestrate various signaling and functional events, including inflammation and immune response[17,18]. Upon activation, various receptors and adaptor molecules are recruited to lipid rafts, which serve as a platform for the inflammatory signaling cascade, including toll-like receptor-dependent signaling[19], interferon signaling[20], interleukin signaling[21], and tumor necrosis factor (TNF) signaling[22]. Given the pivotal role of lipid rafts in the pathogenesis of various pathological conditions, a number of experimental therapies targeting lipid rafts have been reported. However, in retina microglia, the mechanisms of inflammatory signaling events through lipid rafts and the therapeutic approach targeting lipid rafts in retinal microglia have yet to be studied.

Oxysterols, bioactive lipids derived from cholesterol, regulate cholesterol homeostasis and various cellular processes, including inflammation[23–25]. In the normal retina, oxysterol homeostasis is tightly controlled; however, oxysterol levels are profoundly altered during disease states that involve disease progression[26]. In terms of effects, 7-ketocholesterol, the most abundant oxysterol present in the retina, has been described as pro-inflammatory. In contrast, other oxysterols, such as 24(S)-hydroxycholesterol and 25-hydroxycholesterol (25-HC), has been shown to exert anti-inflammatory effects[27–30]. Recent studies highlight the implication of oxysterols in signal transduction through their involvement in lipid raft formation. 7-ketocholesterol has been observed to either promote or inhibit the formation of ordered phase[31], while 25-HC inhibits the formation of membrane lipid rafts in lung epithelial cells and brain microglia[27,32]. Given that each cell type of the cell membrane has a specific sterol and protein composition of lipid raft domains[33], the effects of each oxysterol could be complex and cell type-dependent. Nevertheless, there is currently only a limited body of evidence pertaining to the involvement of oxysterols in the formation of lipid rafts and the subsequent inflammatory signaling pathways in the retina.

Herein, we report that microglia can be activated under simulated μG (SMG) conditions and that they contribute to the acceleration of SMG-induced retinal damage. Using a 3D-SMG device, we confirmed that the early stage of retinal damage can activate microglia, which subsequently contributes to retinal pigment epithelium (RPE) dysfunction and ocular neuronal death in a coculture system and an ex vivo model. Intriguingly, we found that treatment with 25-HC negatively regulates microglial activation through the disruption of membrane lipid rafts formation, which in turn leads to a reduction in secondary retinal injury. Our study introduces a plausible model that links retinal microglial activation to retinal damage under μG conditions. In addition, 25-HC is proposed as a promising candidate drug for the treatment of μG-induced retinal damage by suppressing microglial activation.

Results

SMG exacerbates retinal degeneration

To evaluate retinal damage under SMG conditions, the enucleated mouse globes were collected immediately after sacrifice and then incubated under 1G or SMG conditions for 1, 7, or 14 days (Fig. 1a). Under SMG conditions, retina hematoxylin and eosin staining of the eye sections revealed a reduction in the cell number in the ganglion cell layer, irregular arrangement of cells in the outer nuclear layer (ONL), and a reduction in the retinal layer thickness. No significant abnormalities were observed in the 1 G condition (Fig. 1b, c). To confirm retinal cell death, we performed a TUNEL assay on retinal sections from each group. The SMG-incubated eyes exhibited increased ONL apoptosis, whereas mild ONL apoptosis was detected in the 1G-incubated eyes. These results suggest that μG contributes to and accelerates retinal degeneration (Fig. 1d, e).

SMG induces microglial activation and migration to the injury site

Sustained activation of microglia and a switch to the inflamed phenotype are associated with retinal damage. Recent studies have suggested the possibility that microglial activation is involved in μG-induced retinal damage[34]. Because we observed that retinal damage was increased by SMG, we hypothesized that microglia could be activated by SMG, followed by accelerated irreversible retinal damage. To this end, we first conducted transwell chemotaxis assays using RAW264.7 macrophages, a widely utilized model for innate immune responses due to their shared functional characteristics with microglia, including phagocytic activity and inflammatory signaling pathways. The RCM from the 1G-treated or SMG-treated ARPE-19 cells was placed in the bottom chamber, and the RAW264.7 macrophage cells were seeded in the top chamber; the migratory potential of the RAW264.7 cells was subsequently observed. Compared with the RCM from the 1G-treated ARPE-19 cells, the RCM from the SMG-treated ARPE-19 cells produced significantly greater RAW264.7 cell migration (Fig. 2a–c and Fig. S1a), indicating that microglia can respond to soluble signals and migration toward them. To assess the Raw264.7 cell activation further, coculture experiments were conducted. Flasks containing RAW264.7 macrophage cell strips with or without ARPE-19 cells were incubated under 1 G or SMG for 3 days (Fig. 2d), whereafter the transcript level of the inflammatory genes was examined via reverse transcription (RT)-qPCR. The expression of inflammatory genes in the coculture was higher than that in the RAW264.7 cell monoculture under SMG. However, under 1 G, no significant difference was observed between the RAW264.7 cell monoculture and the coculture with the ARPE-19 cells (Fig. 2e). Raw264.7 cell activation was further confirmed via immunostaining with CD68, an activated microglial marker[35]. We observed that in the SMG-incubated coculture, CD68 expression was prominent, and the RAW264.7 cell morphology changed to a more ramified shape (Fig. 2f, g). These results suggest that early pathological changes in RPE under μG conditions drive the recruitment and activation of Raw264.7 cells.

Previous studies have demonstrated that RPE cells possess intrinsic innate immune capacity. To further investigate their contribution to immune activation under SMG conditions, we analyzed the expression of key innate immunity–related genes in RPE cells. Specifically, we examined the transcript levels of *Nlrp3*, *Nfkb*, and *Il1a*, which are central mediators of inflammasome activation and pro-inflammatory cytokine signaling. Under SMG exposure, all three genes were upregulated in RPE cells. Notably, when RPE cells were cocultured with microglia, their expression was further enhanced (Fig. S1b), indicating a potentiation of the innate immune response. These results suggest that SMG induces a pro-inflammatory state in RPE cells, which may act to recruit and activate microglia, thereby establishing a feedforward inflammatory loop that exacerbates retinal damage.

Microglia exacerbate retinal damage following SMG

Given that μG-induced stress in RPE cells can promote microglial activation, we subsequently examined whether microglia aggravate retinal damage. To this end, we first investigated RPE damage and activation in monoculture or coculture with microglia. Under SMG, we observed that the transcript level of inflammatory genes in the RPE increased in coculture with microglia (Fig. 3a). Since RPE is involved in maintaining the outer blood–retina barrier (BRB), and supports the functional integrity of the retina[36], we sought to determine whether microglial activation involves the RPE barrier function. The level of the tight junction marker ZO-1[37] and the levels of MMP-9 and VEGF—which are involved in barrier breakdown[38,39]—were measured via western blotting.

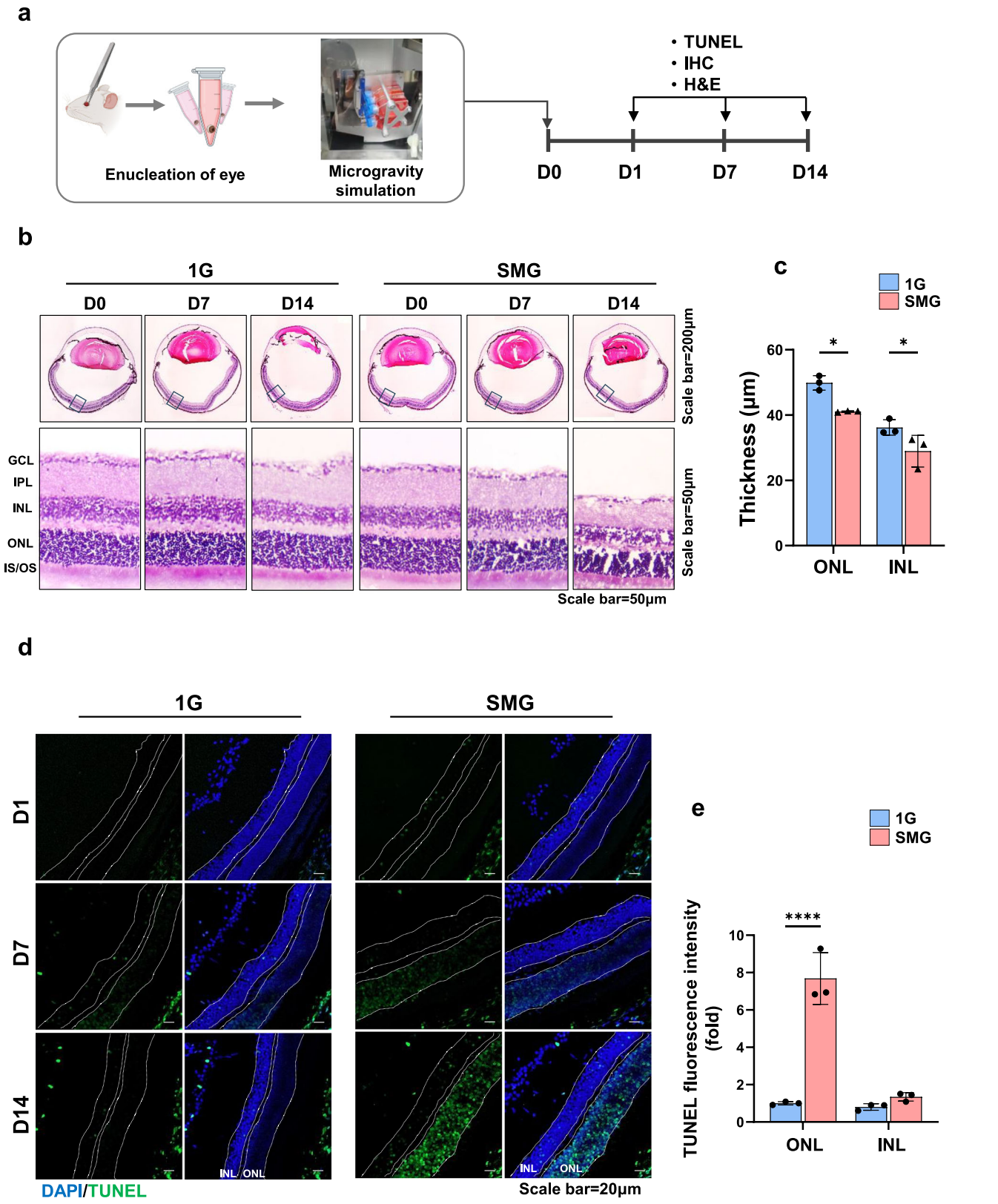

Fig. 1 | Simulated microgravity accelerates retinal degeneration. a Schematic of the experimental design. The mouse globes were cultured under normal 1 G or 10^{-3}G microgravity conditions using a 3D clinostat device for 14 days.Representative hematoxylin and eosin-staining images of retinal sections from 1G-treated or SMG-treated mouse globes (**b**). Summary data showing thickness of retinas on Day 14 (**c**). Representative images (**d**) and summary data (**e**) showing TUNEL staining of retina sections from 1G-treated or SMG-treated mouse globes. All data are representative of three fields of view per group of three independent experiments. Data are presented as mean ± SD (*$p < 0.05$, ****$p < 0.0001$). INL, inner nuclear layer; ONL, outer nuclear layer. *P* values displayed above the graphs were calculated using an unpaired two-tailed Student's *t*-test. Image created with BioRender.com.

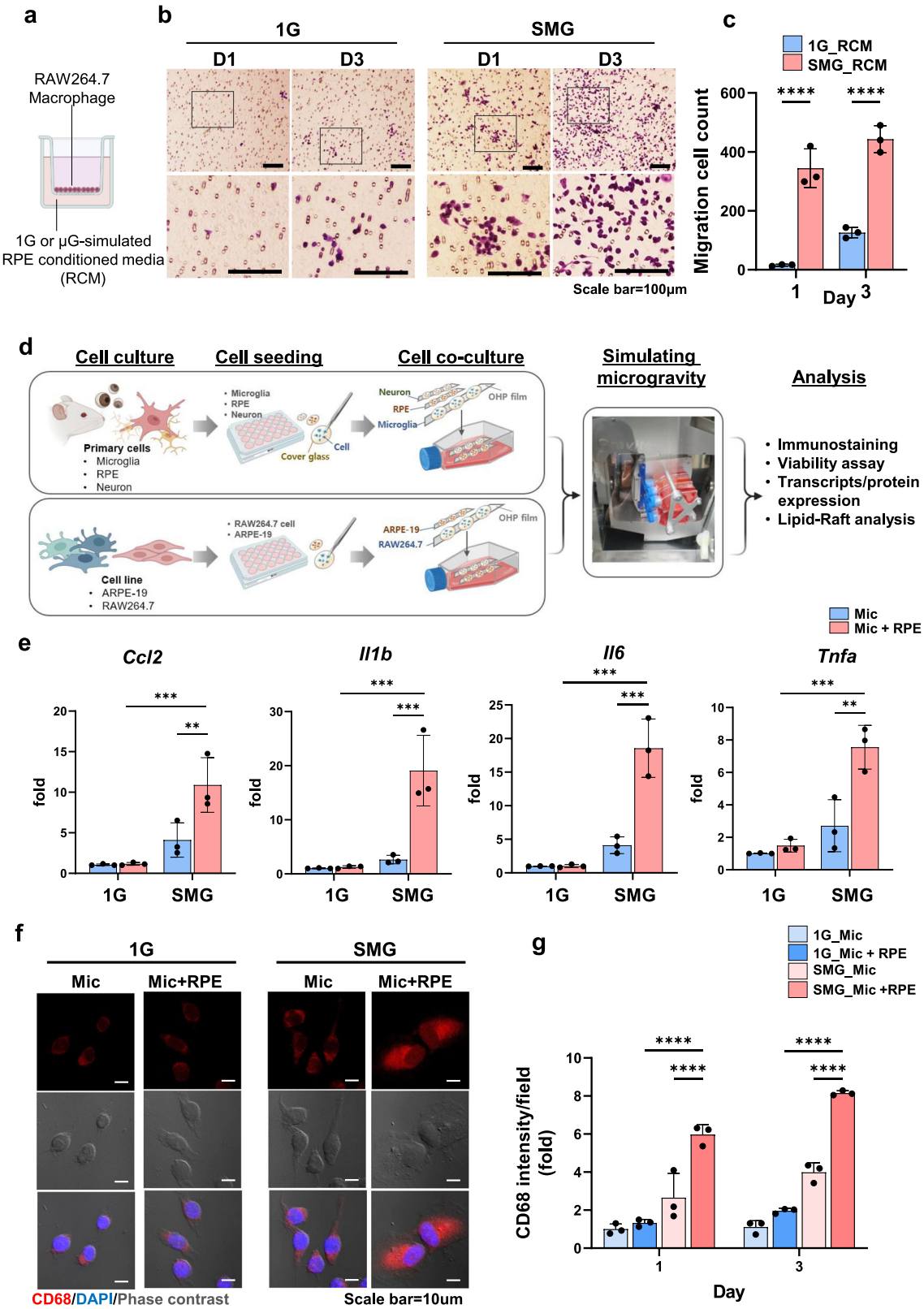

Fig. 2 | Simulated microgravity induces retinal microglial activation. a Schematic representation of transwell chemotaxis assay. Representative images (**b**) and analysis (**c**) of RAW264.7 macrophage migration toward conditioned medium from ARPE-19 RPE cells cultured under 1G or SMG. The data are representative of three fields of view per group of three independent experiments. Data are presented as mean ± SD (**$p < 0.01$, ***$p < 0.001$). **d** Schematic of experimental design. RAW264.7 cells cocultured with or without primary RPE were incubated under 1 G or SMG. **e** Transcript levels of inflammatory genes in microglia examined via RT-qPCR. Data are expressed as mean ± SD from three independent experiments (**$p < 0.01$, ***$p < 0.001$. **f** Representative confocal images of CD68 in RAW264.7 cells cultured with or without primary RPE. **g** Summary data showing CD68 staining. Data are representative of three fields of view per group of three independent experiments. Data are presented as mean ± SD (***$p < 0.001$, ****$p < 0.0001$). *P* values displayed above graphs were calculated using one-way ANOVA (in **c**) or two-way ANOVA for multiple comparisons (in **e**). Image created with BioRender.com.

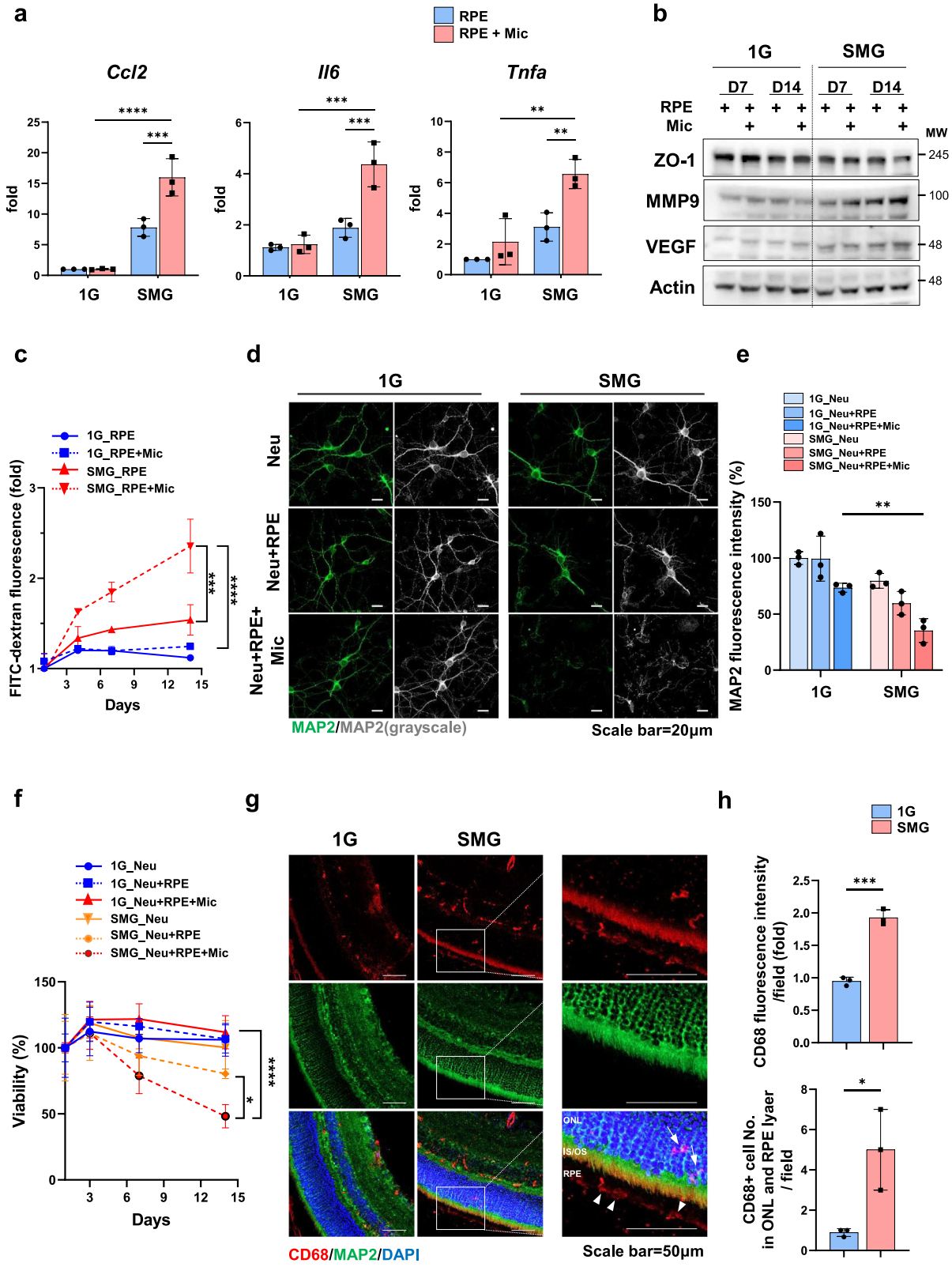

In the coculture with microglia, the ZO-1 levels were reduced, whereas the VEGF and MMP-9 levels were increased (Fig. 3b and Fig. S1c). To confirm the role of microglia in altering the barrier function of RPE, we measured the change in the permeability of the RPE layer to FITC–dextran flux. The RPE cocultured with microglia was more permeable to FITC–dextran under SMG than under 1G (Fig. 3c). We also observed that the presence of microglia slightly reduced the viability of RPE under SMG, but this effect was not significant (Fig. S1d). These findings suggest that SMG-induced activation of RPE cells leads to the release of soluble chemoattractants, which in turn promote microglial recruitment and activation. This bidirectional interaction likely forms a feedforward inflammatory loop, wherein activated microglia further

Fig. 3 | Microglial activation by simulated microgravity exacerbates retinal damage. Primary RPE cells cultured with or without microglia under 1 G or SMG. After 7 or 14 days, the transcript levels of inflammatory genes in RPE were examined via RT-qPCR (**a**), and the levels of the indicated proteins were measured via western blotting (**b**). Data are expressed as mean ± SD from three independent experiments (**$p < 0.01$, ***$p < 0.001$, ****$p < 0.0001$). **c** Permeability of RPE cells with or without microglia measured through FITC–dextran leakage assay for 14 days. The graph presents the mean ± SD from three independent experiments (***$p < 0.001$, ****$p < 0.0001$). Primary retinal neurons cultured with or without microglia and RPE cells, incubated under 1 G or SMG for 14 days. Representative immunofluorescence images (**d**) and summary data (**e**) showing MAP-2 staining. Data are representative of three fields of view per group of three independent experiments and are presented as mean ± SD (**$p < 0.01$). **f** Graph showing the percentage of viable primary neurons cultured with or without microglia or RPE cells, as measured via WST-8 assay. Results are presented as mean ± SD from three independent experiments (*$p < 0.05$, ****$p < 0.0001$). Mouse globes were exposed to normal 1 G or SMG for 14 days, and then retinal sections were subjected to immunohistochemistry with the indicated antibodies. Representative confocal images (**g**) and summary data showing the intensity of CD68 (left) and the number of CD68-positive cells in the ONL and RPE (right) (**h**). The microglia located in the ONL and RPE are indicated by arrows and arrowheads, respectively. Data are representative of three fields of view per group of three independent experiments, presented as mean ± SD (*$p < 0.05$, ***$p < 0.001$). *P* values displayed above graphs were calculated using unpaired two-tailed Student's *t*-test (in h) or two-way ANOVA for multiple comparisons (in **a**, **c** and **e**).

exacerbate RPE dysfunction, collectively accelerating retinal degeneration under SMG conditions.

We also observed that the neurite length and the percentage of cells positive for MAP-2, a mature neuron marker, in the microglial coculture were lower than those in the retinal neuron monoculture (Fig. 3d, e). Concurrently, viability assays revealed that microglial activation was responsible for the death of retinal neurons (Fig. 3f). In an ex vivo eye organotypic culture, disrupted neuronal organization was observed under SMG, as revealed by MAP-2 staining of retinal vertical sections (Fig. S1e). This abnormal arrangement of retinal neurons was accompanied by CD68-positive microglial migration to the ONL and RPE layers (Fig. 3g, h). Overall, μG induces microglial activation and migration, leading to further retinal damage.

25-HC suppressed microglial activation

The foregoing results inspired us to search for inhibitory molecules capable of suppressing retinal microglial activation. Recent evidence suggests that 25-HC inhibits neurodegenerative disease by suppressing brain microglial activation[27]. Therefore, although this has not been extensively researched with regard to retinal microglia, we hypothesized that 25-HC could suppress retinal microglial activation. To examine the effect of 25-HC, we treated microglia in the presence or absence of RPE or neurons with 25-HC under 1G or SMG. While 25-HC suppressed the SMG-induced expression of inflammatory genes at a low concentration (5 μM), it either increased or had no further suppressive effect on the expression of inflammatory mediators in concentrations greater than 10 μM (Fig. 4a and Fig. S2a). Consistent with these findings, we also observed that 25-HC inhibited the CD68-positive activated Raw264.7 cell phenotype (Fig. 4b, c). To determine whether this effect was direct, we conducted experiments using RAW264.7 cell monocultures treated with or without 25-HC under both 1 G and SMG conditions. In monocultures, 25-HC at low concentrations (5–10 μM) effectively reduced the expression of inflammatory genes and CD68, suggesting a direct anti-inflammatory effect on Raw264.7 cell that may contribute to retinal protection under SMG (Fig. S2c, d). Although various insults are known to increase Ch25h, an enzyme that converts cholesterol into 25-HC, we found that the transcript level of Ch25h was barely affected by SMG stimulation (Fig. S2b). Accordingly, we rule out the possibility that endogenous 25-HC could involve retinal damage under SMG.

25-HC suppress inflammatory signaling in microglia by disrupting lipid raft formation

A number of inflammatory signaling processes in cells are regulated by compartmentalization of receptors in raft domains; therefore, disruption of lipid rafts could result in the attenuation of the inflammatory response in retinal microglia. Since recent study suggest that 25-HC inhibits inflammatory signaling in brain microglia by disrupting lipid raft formation[27], we postulated that 25-HC could suppress SMG-induced retinal microglia activation by influencing lipid raft formation. To test this hypothesis, we first examined whether SMG affects the trafficking of inflammatory cytokine receptors to the lipid raft fraction and whether 25-HC inhibits this process in retinal microglia. By sucrose density gradient centrifugation, which is used to isolate lipid microdomains, we observed that various cytokine receptors, such as TNF receptor1 (TNFR1) and IL-6 receptor alpha (IL-6Rα), were detected in the raft fraction under SMG conditions, but were significantly reduced in the raft fraction by 25-HC treatment (Fig. 5a). These results indicate that in response to SMG stimulation, receptors involved in the inflammatory response localized and activated within lipid raft microdomains, and that 25-HC inhibits this process by disrupting lipid raft formation. To further examine these findings, we performed colocalization of inflammatory receptors and green fluorescence protein-domain D4 (GFP-D4), a cholesterol-binding protein used as a molecular imaging marker for lipid rafts. In the SMG condition, clustering of D4-positive lipid raft microdomains containing IL-6Rα was increased, which was suppressed by treatment with 25-HC (Fig. 5b). To confirm these results, we then examined the SMG-induced lipid raft formation with a widely used lipid-soluble fluorescent probe, trimethylammonium diphenylhexatriene (TMA-DPH). In the SMG condition, the formation of TMA-DPH-positive puncta in microglia was increased, which was attenuated by treatment with 25-HC (Fig. S2e). These findings collectively suggested that 25-HC inhibits the inflammatory response in microglia by disrupting lipid raft formation.

25-HC ameliorates SMG-induced retinal damage by suppressing microglial activation

Next, we assessed the efficacy of 25-HC in preventing damage to RPE cells and retinal neurons. RPE cells were treated with 25-HC, before being incubated under 1 G or SMG conditions. We observed that 25-HC suppressed the transcript level of inflammatory genes and reversed the expression of proteins involved in the RPE barrier function (Fig. 6a, b; Fig. S3a, b). Notably, the elevated ROS levels observed under SMG conditions were significantly reduced following treatment with 25-HC, suggesting a direct role for 25-HC in alleviating oxidative stress (Fig. S3c). Furthermore, SMG-induced abnormal neuronal morphology and neuronal death were suppressed upon 25-HC treatment (Fig. 6c–e). An ex vivo eye organotypic culture also confirmed that 25-HC ameliorated the SMG-induced abnormal arrangement of retinal neurons and the CD68 expression (Fig. 6f, g). To further evaluate the roles of microglia in retinal damage, eyes were treated with PLX5622, a CSF1R inhibitor that efficiently depletes microglia, followed by incubating under 1 G or SMG in the presence or absence of 25-HC. The expression level of Iba1, a canonical marker for microglia, confirmed that most microglial cells were depleted by PLX5622 (Fig. S3d). In microglia-depleted eyes, SMG-mediated retinal death was attenuated and ONL thinning was reduced compared to microglia-intact eyes. Notably, the protective effect of 25-HC was less pronounced in the absence of microglia, highlighting the pivotal role of microglia in mediating SMG-induced retinal degeneration (Fig. 6h). Together, these results suggest that 25-HC effectively suppresses retinal microglial activation, thereby attenuating μG-induced secondary retinal damage.

Discussion

Understanding the pathogenesis of SANS is important for enabling future human space exploration. Despite many advances, significant knowledge gaps remain in this regard, including the etiology of SANS, treatment

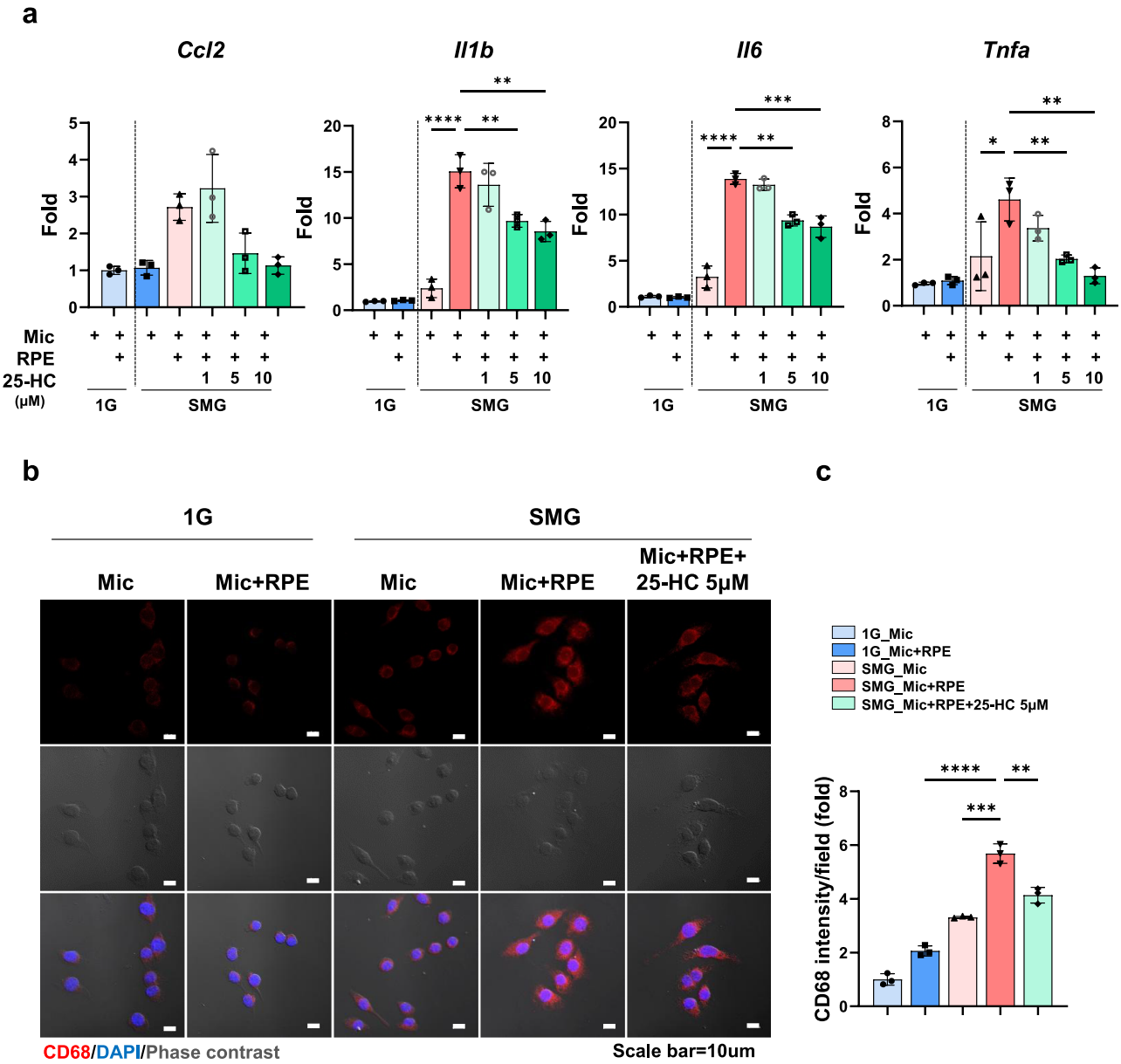

Fig. 4 | 25-HC suppresses simulated microgravity-induced microglial activation. **a** Primary microglia cultured with or without RPE cells were treated with various concentrations of 25-HC under 1G or SMG. After 7 days, the transcript levels of inflammatory genes in microglia were examined via RT-qPCR. Data are expressed as mean ± SD from three independent experiments (*$p < 0.05$, **$p < 0.01$, ***$p < 0.001$, ****$p < 0.0001$). **b** Representative confocal images of CD68 in RAW264.7 cells. **c** Summary data showing CD68 staining. Data are representative of three fields of view per group of three independent experiments and are presented as mean ± SD (**$p < 0.01$, ***$p < 0.001$, ****$p < 0.0001$). *P* values displayed above the graphs were calculated using unpaired two-way ANOVA for multiple comparisons.

strategies, and the development of research systems on the ground, as outlined in reports from the National Aeronautics and Space Administration and the European Space Agency[40,41]. Herein, we highlight the significant role of microglia in ocular degeneration under SMG. Following SMG-induced primary retinal damage, microglia were observed as inflammatory cells, which accelerated secondary ocular damage (Fig. 7).

Despite the important role of microglia in various ocular diseases, changes in their characteristics and function in the context of SMG-induced ocular damage have rarely been studied. In our study, damage to the RPE and retinal neurons was exacerbated in coculture with microglia, whereas minimal damage was observed in monocultures of RPE or neurons. This suggests that microglia constitute a key factor accelerating SMG-induced retinal injury. While our findings indicate a detrimental role for microglia under SMG, it is important to note that these observations were derived from a co-culture system. Although such reductionist approaches allow for precise dissection of microglia–retina interactions, they do not fully recapitulate the complex immune landscape of the intact organism. In particular, they lack systemic influences and cannot distinguish between resident microglia and infiltrating monocyte-derived macrophages, both of which can exhibit distinct and sometimes opposing roles in neuroinflammation[42–45]. To address this, we employed PLX5622, a selective CSF1R inhibitor that depletes resident microglia[46], and observed significant attenuation of SMG-induced retinal injury. This finding reinforces the central role of resident microglia in this process. Notably, PLX5622 has also been shown to suppress the repopulation of resident microglia/macrophages during treatment, as demonstrated in prior studies[47]. Although the short duration of PLX5622 administration in our study likely minimized its impact on the outcomes, this remains a potential limitation. Future in vivo and in vitro studies will take this into account in the design of microglia-targeting strategies. Furthermore, we acknowledge that our current model cannot fully recapitulate peripheral immune contributions. To address this limitation, future in vivo studies employing lineage tracing and fate-

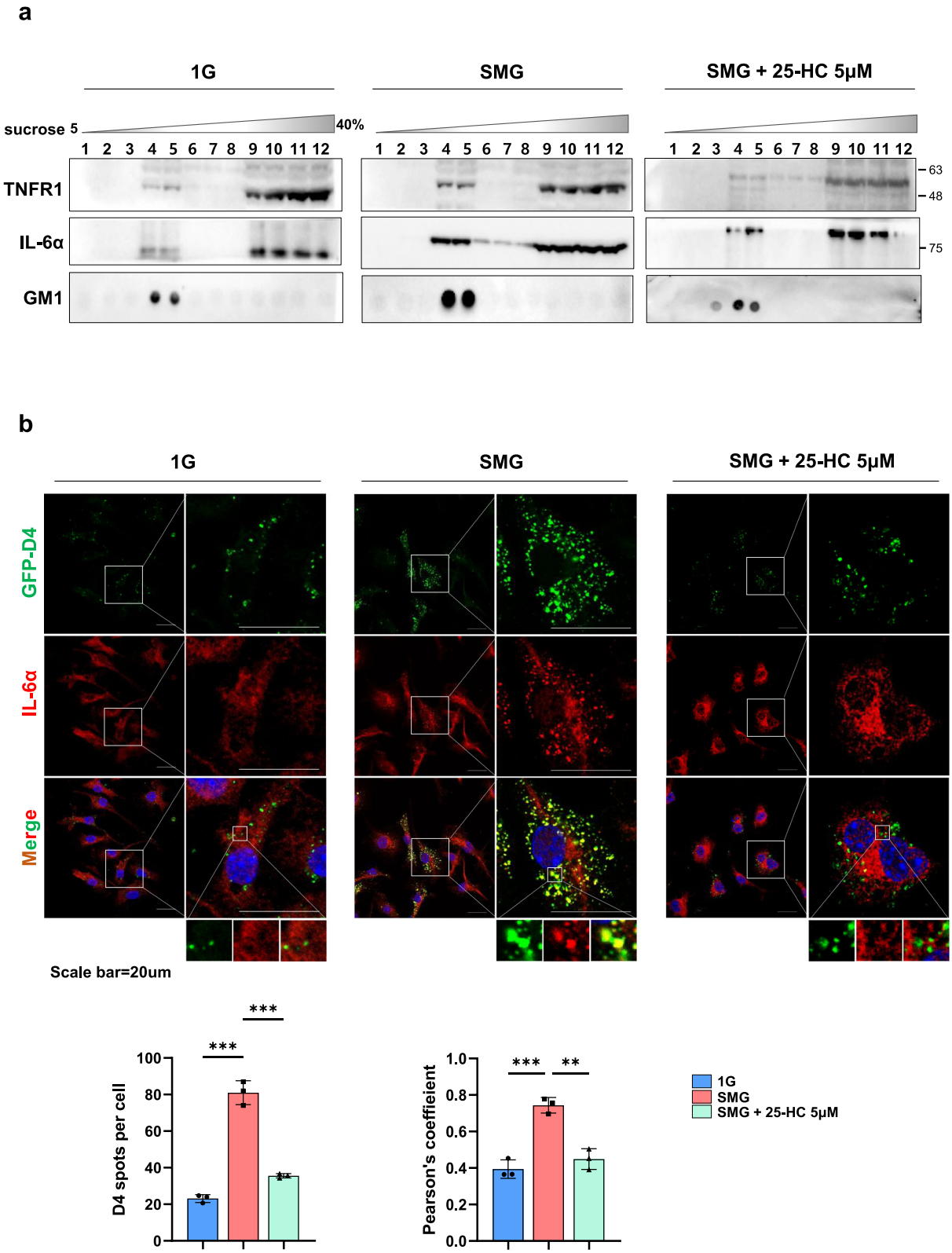

Fig. 5 | 25-HC disrupted lipid raft formation to suppress the inflammatory response in microglia. a Lysates from the retinal microglia were subjected to sucrose gradient centrifugation. Twelve fractions were collected from top to bottom[1–12]. Equal volumes of each fraction were pooled together and subsequently subjected to western bolt analysis using the indicated antibodies. GM1 was detected using HRP-labeled CT-B. **b** Representative confocal images of primary microglia labeled with GFP-D4 protein. Total average number of GFP-D4 puncta (lower left graph) and colocalization rate of GFP-D4 puncta with IL-6Rα (lower right graph). Data are representative of three fields of view per group of three independent experiments. Scale bar, 20 μm. All data are presented as mean ± SD. $^{***}p < 0.001$, $^{**}p < 0.01$. *P* values displayed above graphs were calculated using unpaired one-way ANOVA for multiple comparisons.

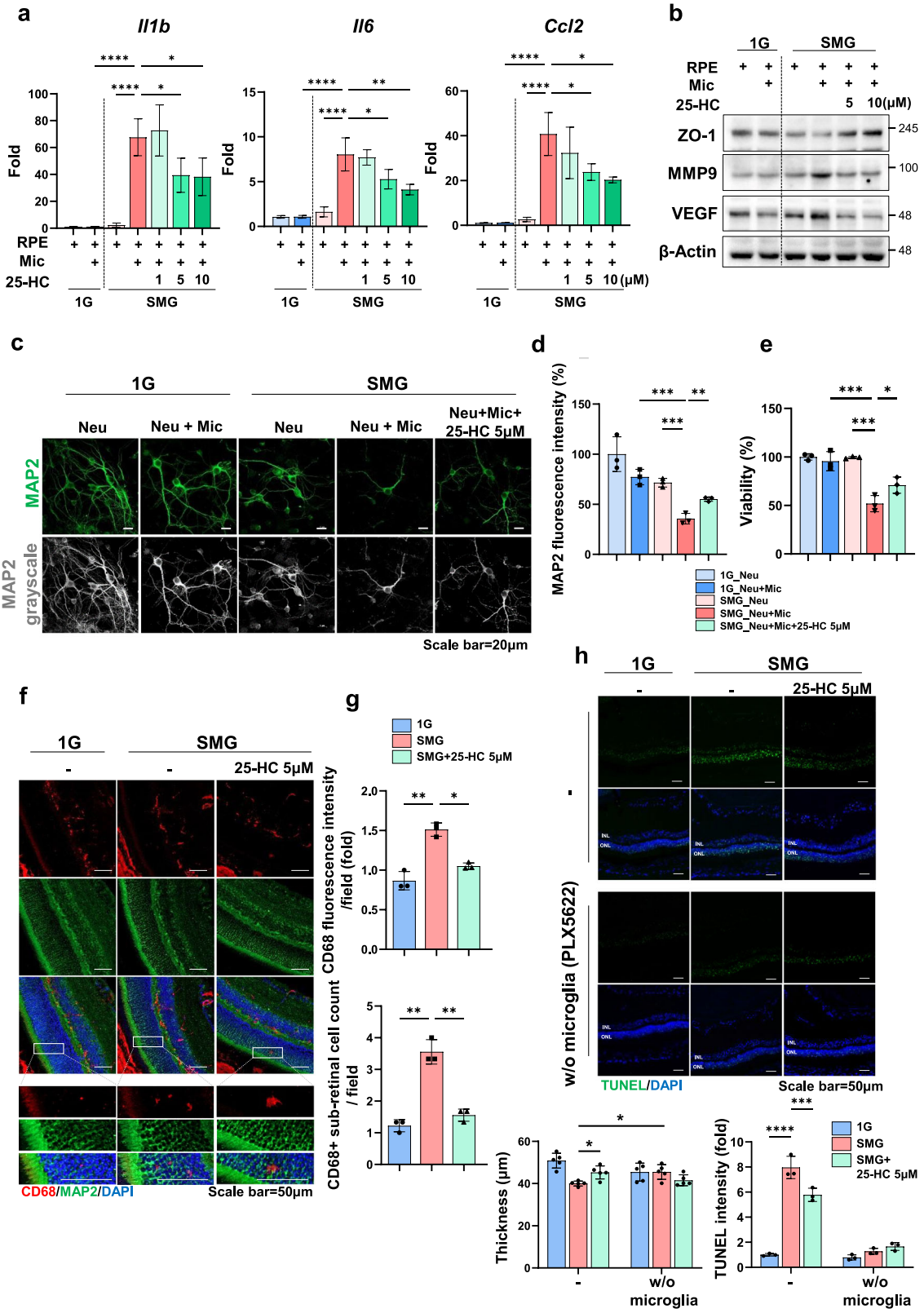

mapping approaches will be essential to delineate the respective roles of resident microglia and infiltrating monocyte-derived macrophages, and to better define the immune landscape of the retina under spaceflight conditions.

Interestingly, recent studies have demonstrated that microglia can exert protective functions in models of retinal aging and degeneration, where depletion of microglia worsens disease phenotypes. For example, O'Koren et al. reported that microglia migrating to subretinal space undergo transition reprograming, thereby protecting the RPE from damage[42]. In models of AMD, microglia have been shown to support RPE function, and a conserved subset of calactin-3-expressing microglia was identified as protective against retinal degeneration[43,48]. These findings underscore the

Fig. 6 | 25-HC ameliorates simulated microgravity-induced retinal damage. Primary RPE cells cultured with or without microglia were treated with various concentrations of 25-HC under 1 G or SMG. After 7 or 14 days, the transcript levels of inflammatory genes in RPE were examined via RT-qPCR (**a**), and the levels of the indicated proteins were measured via western blotting (**b**). Data are expressed as mean ± SD from three independent experiments (*$p < 0.05$, **$p < 0.01$, ****$p < 0.0001$). Primary retinal neurons cultured with or without microglia were treated with 25-HC under 1 G or SMG for 14 days. Representative immunofluorescence images (**c**) and summary data (**d**) showing MAP-2 staining. Data are representative of three fields of view per group of three independent experiments and are presented as mean ± SD (*$p < 0.05$, **$p < 0.01$, ***$p < 0.001$). **e** Graph showing the percentage of viable primary neurons as measured via WST-8 assay. Results are presented as mean ± SD from three independent experiments (*$p < 0.05$, ***$p < 0.001$). 25-HC-treated mouse globes were exposed to 1 G or SMG for 14 days, and retinal sections were then subjected to immunohistochemistry with the indicated antibodies. Representative confocal images (**f**) and summary data showing the intensity of CD68 (top) and the number of CD68-positive cells in the ONL and RPE (bottom) (**g**). **h** TUNEL staining of retinal sections from mouse eyes treated with vehicle or PLX5622, with or without 25-HC, under the indicated experimental conditions. Representative TUNEL-stained images are shown (top). Quantification of TUNEL-positive cells is presented (lower right graph), and ONL thickness is summarized as a bar graph (lower left graph). All data are representative of three fields of view per group of three independent experiments and are presented as mean ± SD (*$p < 0.05$, **$p < 0.01$, ***$p < 0.001$, ****$p < 0.0001$). *P* values displayed above graphs were calculated using unpaired two-tailed Student's *t*-test (in g) or two-way ANOVA for multiple comparisons (in **a**, **d**, **e**, **h**).

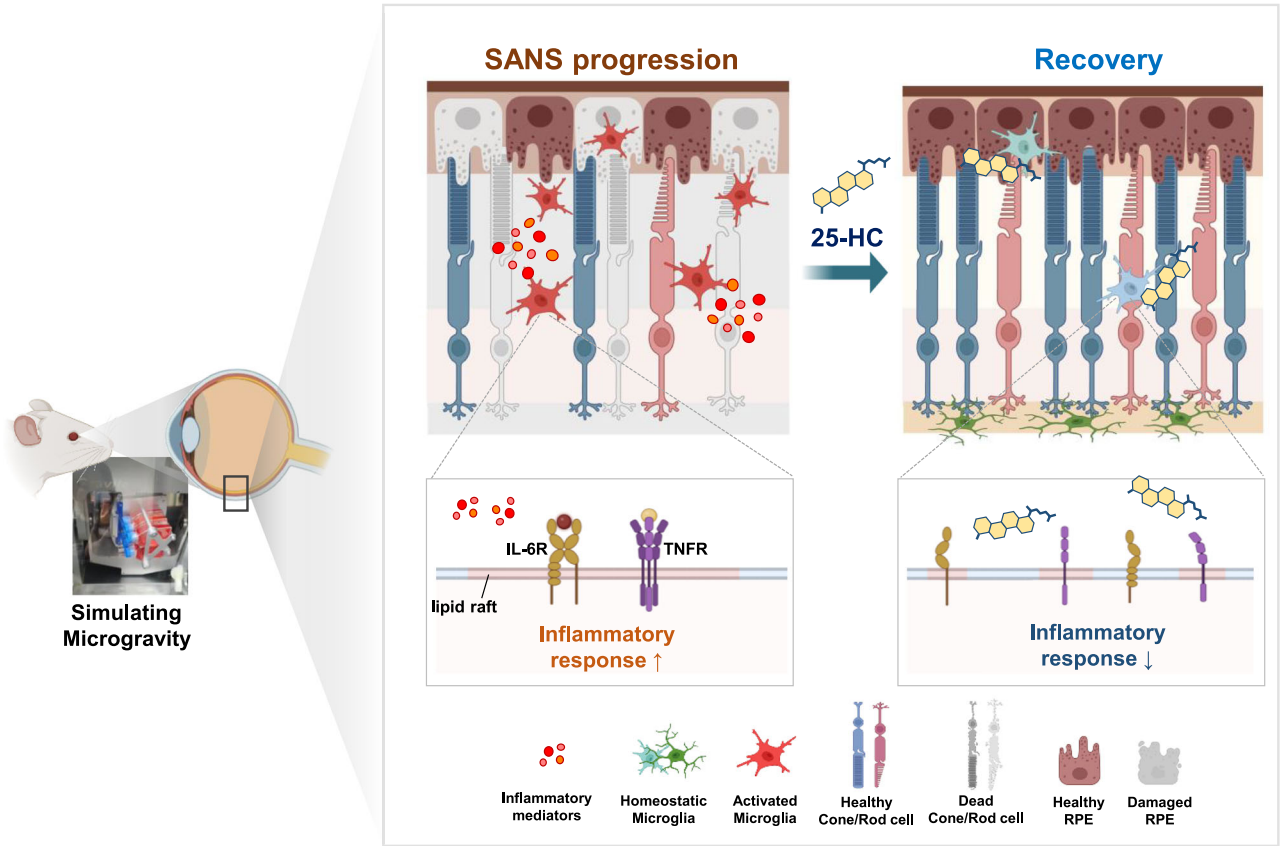

Fig. 7 | Schematic of simulated microgravity-induced microglial activation and the anti-inflammatory effects of 25-HC. As an initial response to μG, RPE cells express various inflammatory mediators, which, in turn, cause microglial activation. Activated microglia migrate to the damage site, causing persistent and excessive inflammation, which accelerates RPE cell damage and neuronal cell death. A low dose of 25-HC suppress inflammatory response in microglia by disrupting lipid raft formation and thereby mitigates the severity of SANS. Image created with BioRender.com.

context-dependent nature of microglial function. In contrast, our data suggest that under SMG conditions, microglia adopt a pro-inflammatory and neurotoxic phenotype, contributing to the progression of retinal damage. This discrepancy highlights the need for comprehensive transcriptomic profiling of SMG-exposed microglia to determine whether their molecular signatures align more closely with disease-associated or homeostatic microglial states. Therefore, in vivo studies will be essential to validate our findings within the context of whole-organism immune dynamics. Additionally, transcriptional analyses-particularly those that focus on microglial reprograming-will be essential for elucidating the unique microglial phenotypes induced by microgravity and comparing them with those seen in other models of retinal degeneration.

Beyond microglia, Müller glial cells (MGCs) may also contribute to SMG-induced retinal damage. Studies using experimental spaceflight models have shown that MGCs undergo reactive gliosis and cytoskeletal remodeling, which may exert both neuroprotective and neurotoxic effects depending on the context[49–51]. In inflamed retinal environments, activated microglia can signal to MGCs and modulate their functional states[52–54]. However, the precise mechanisms governing microglia–MGC crosstalk remain incompletely understood. Given the essential roles of MGCs in maintaining retinal homeostasis—including the integrity of the inner BRB[55], neuronal support[56], and immunoregulation[57]—deciphering the bidirectional interactions between microglia and MGCs will be key to understanding and ultimately mitigating ocular damage caused by spaceflight-associated environmental stress.

Oxysterols, which are oxidized cholesterol derivatives, regulate various cellular processes and disease mechanisms, including those involved in neurodegenerative disorders and ocular disease[24,26,58]. In the retina, oxysterol

homeostasis is tightly controlled by pathways regulating cholesterol biosynthesis, cholesterol efflux, and enzymatic biotransformation[59]. However, under pathological conditions, oxysterol levels are altered, which has been linked to ocular degeneration. In this regard, 7-KC, the most abundant form of oxysterol found in the retina, contributes to the production of ROS and pro-inflammatory mediators and induces cell death in age-related macular degeneration (AMD)[60,61]. In contrast, 27-hydroxycholesterol may play a protective role in the pathogenesis of AMD through its involvement in translocator protein-mediated cholesterol trafficking[62,63]. Although reports indicate that 25-HC increases ROS in RPE cells[64,65], it is also known to have anti-inflammatory effects on brain glial cells and macrophages[27–30]. Despite the discovery of such roles of oxysterols in ocular damage, the effect of oxysterols on the pathophysiology of SANS remains unknown. In this study, we discovered that 25-HC has anti-inflammatory effects on microglia under SMG. However, high concentrations of 25-HC (> 10 μM) increase the inflammatory response in microglia (Fig. S2a), suggesting that the abundance of 25-HC in SANS states could be considered a determinant of its pro-inflammatory or anti-inflammatory effects. Some reports indicate that the level of 25-HC is increased under ocular damage conditions and that elevated 25-HC concentrations (50–155 μM) can contribute to RPE cell death[64,66,67]. Additionally, in neurodegenerative disease, 25-HC can play either neuroprotective roles or contribute to disease exacerbation, depending on its concentration range[68]. Since the concentration of 25-HC varies between disease states, the function of 25-HC in ocular damage should be considered on the basis of the specific etiology and type of ocular disease. Herein, we suggest that low doses of 25-HC reduce the SMG-induced inflammatory response of microglia, thereby mitigating damage to the RPE and neurons. Further investigation is required to identify the changes in 25-HC concentration in the retina at each stage of spaceflight (pre-flight, in-flight, and post-flight) and to assess the impact of 25-HC on the biological processes of each cell type in the retina and the progression of SANS. Our findings confirmed that inflammatory microglia exacerbate SMG-induced retinal damage. These findings further suggest that microglia play significant roles in SANS pathology and can be targeted for the development of novel therapeutics. Many studies have reported strategies for targeting the inflammatory response mediated by microglia or for modifying microglia[69,70]. Replenishing healthy microglia using stem cell therapy or removing dysfunctional microglia could be suitable strategies for treating SANS; however, further evaluation is necessary to determine the ideal timing of microglial depletion or addition depending on the SANS stage. Although various drugs that target microglial inflammatory responses, such as nonsteroidal anti-inflammatory drugs or inflammasome inhibitors, have also been reported to be effective, whether they have distinct clinical effects remains unclear. Furthermore, membrane impermeability due to the BRB and the metabolic destruction of drugs pose significant challenges in drug discovery for targeting microglia[66,71]. Given the limitations of existing strategies targeting microglia, leveraging the anti-inflammatory effects and BRB-penetrating capability of 25-HC in microglia represents a promising therapeutic strategy for mitigating retinal damage during spaceflight.

Methods

Cell culture

Primary retinal microglia were cultured from 1-day-old C57BL/6 mice from female (Orient Bio, Korea). In brief, the eyes were removed and placed in ice-cold Hank's buffered salt solution (HBSS; Welgene, Korea) supplemented with N-2-hydroxyethylpiperazine-N'-2-ethanesulfonic acid (HEPES, 10 mM, pH 7.4). To preserve the retinas, the corneas were cut away, and the crystalline lens and pigment epithelium layer were removed. The retinas were triturated into single cells in Dulbecco's modified Eagle's medium (DMEM; Welgene) containing 10%(v/v) fetal bovine serum (FBS; HyClone, South Logan, UT) and penicillin/streptomycin (1%), before being plated onto poly-D lysine (1 mg/mL)-coated 75 cm^2 T-flasks for 2 weeks. The microglia were detached from the flask by shaking it and were filtered through a nylon mesh to remove other cells and clumps. The microglia were then counted and plated onto 25 cm^2 T-flasks, cover glasses, or transwells at an appropriate density.

Primary neurons were cultured as described above. In brief, the retinas were triturated and incubated in HBSS containing trypsin (0.05%; Welgene) and DNase I (100 μg/mL; Sigma, St. Louis, MO) for 15 min at 37 °C, before being dissociated via gentle pipetting. The dissociated cells were plated onto poly-D-lysine-coated 12 mm cover glass or 96-well plates in Neurobasal medium containing B27 (2%), sodium pyruvate (1%), penicillin/streptomycin (1%), and GlutaMAX (1%) (all supplements were from Gibco, Carlsbad, CA) for 7 days.

Primary RPE cells were cultured from 5–6-month-old wild-type male C57BL/6 mice. The cornea and lens were removed, and the RPE layer was carefully peeled from the retinas. The RPE layer was subsequently incubated with trypsin for 10 min at 37 °C and then dissociated through gentle pipetting. The dissociated cells were plated onto 25 cm^2 flasks, transwells, or 96-well plates in DMEM containing FBS (10%) and penicillin/streptomycin (1%). For the experiments, the media were changed to lower the FBS concentration to 1% when the cells were fully confluent.

Human retinal pigment epithelial ARPE-19 cells, which were derived from the normal eyes of a healthy 19-year-old male donor and RAW264.7 macrophages, a murine macrophage cell line originating from a male BALB/c mouse leukemia, were obtained from ATCC (Manassas, VA).The cells were plated onto tissue-culture plates in DMEM containing FBS (10%) and penicillin/streptomycin (1%). ARPE-19 cells were used between passages 19 and 22, while RAW264.7 cells were used between passages 25 and 27. When the ARPE-19 cells were fully confluent, the medium was changed to DMEM supplemented with 1% FBS and 1% GlutaMAX. After 4 weeks, the ARPE-19 cells formed a regular cobblestone monolayer.

For coculture with multiple types of cells, the RPE, microglia, and neurons were seeded on 12 mm coverslips and attached to transparent thin plastic film strips using safe and nontoxic ethylene vinyl acetate glue. To simulate μG, the cell strips were inserted into 25 cm^2 T-flasks containing DMEM (with 10% FBS and 1% penicillin/streptomycin) and then cultured under 1G or 10^{-3}G conditions for up to 14 days. All experimental procedures were approved by the Institutional Animal Center and Use Committee of Inha University (INHA 240214-912).

Organotypic culture

Organotypic eye cultures were prepared from adult C57BL/6 mice following previously reported protocols[72] with minor modifications. In brief, the mice were anesthetized, and the eyes were enucleated. Subsequently, the eyes were placed in HBSS containing HEPES (10 mM), and the meningeal sheath surrounding the optic nerve was carefully removed. To simulate μG, the enucleated globes were placed in 0.5 mL microtubes—filled completely with Neurobasal medium containing B27 (2%), sodium pyruvate (1%), penicillin/streptomycin (1%), and GlutaMAX (1%)—and then incubated under 1G or 10^{-3}G conditions for up to 14 days. During SMG, the culture medium was changed every 2–3 days. All animal experiments were approved by the Institutional Animal Care and Use Committee (IACUC) of Inha University (Approval No. INHA-240214-912) and were conducted in accordance with the guidelines for the care and use of laboratory animals established by the committee.

Microgravity simulation

To simulate μG, the cells or globes were cultured under normal 1 G or 10^{-3}G conditions using a Gravite® device (Space Bio-Laboratories, Japan). This device produces an environment replicating spaceflight conditions (10^{-3} G) by 3D-rotating a sample around two axes[73,74]. To avoid fluid shearing, the cell culture flasks or tubes were carefully filled with the culture medium, ensuring that no bubbles were formed. The flasks or tubes were placed on the Gravite® device, and microgravity was induced in Mode C (×2 rpm), as recommended for cell culture. The Gravite® device was operated in a CO_2 incubator at 37 °C and 5% CO_2. The culture media were changed every 2–3 days for up to 14 days.

Real-time reverse transcription–quantitative polymerase chain reaction analysis

Total RNA was isolated using RNAiso Plus (TaKaRa, Japan), and cDNA was synthesized using Moloney murine leukemia virus reverse transcriptase and oligo (dT) (CellSafe, Korea), in accordance with the manufacturer's instructions. For the quantitative polymerase chain reaction (qPCR), amplification reactions were performed using a CFX real-time PCR system (Bio-Rad, Hercules, CA) with the SYBR qPCR master mix (CellSafe), as per the manufacturer's instructions. The value of each cDNA was calculated using the ΔCt method and normalized to the value of the housekeeping gene, *Actin*. The primers used for the qPCR (Bioneer, Korea) are described in Table S1.

Western blotting

The cells were lysed with RIPA buffer (50 mM Tris-HCl pH 7.5, 150 mM NaCl, 1% Triton X-100, 1% sodium deoxycholate, 0.1% SDS, and 2 mM ethylenediaminetetraacetic acid at pH 8.0) supplemented with a cocktail of protease inhibitors (ATTO, Japan) at 4 °C for 30 min. The samples were separated using SDS-PAGE and transferred to nitrocellulose membranes. The membranes were incubated with primary antibodies and horseradish peroxidase–conjugated secondary antibodies, and the bands were visualized using an enhanced chemiluminescence system (Bio-Rad). With regard to the primary antibodies, rabbit anti-zonular occludens 1 (ZO-1) and mouse anti-matrix metalloproteinase-9 (MMP-9) were purchased from Thermo Fisher Scientific (Waltham, MA), while mouse anti-vascular endothelial growth factor (VEGF) and mouse beta-Actin were purchased from Santa Cruz (Santa Cruz, CA).

Isolation of lipid rafts by sucrose density gradient ultracentrifugation

The primary retinal microglia were treated with the RPE cell–conditioned medium (RCM) from the 1G- or SMG-treated primary RPE cells. After 2 days, microglia were lysed in lysis buffer (500 mM Na_2CO_3, 25 mM MES, 150 mM NaCl) containing protease inhibitors, and the lysates were sheared through a 23-gauge needle with 20 complete passes. The lysates were adjusted to 45% sucrose, overlayed with 35 and 5% sucrose in lysis buffer. The mixed lysates were centrifuged at 38,000 rpm for 20 hr in a SW55 rotor (L-90K, Beckman-Coulter, Brea, CA). From top of the gradient, twelve 1 ml fractions were collected. To concentrate proteins for western blot analysis, each fraction was subjected to trichloroacetic acid (TCA) precipitation by adding TCA to a final concentration of 10%, followed by incubation on ice for 30 min. The precipitated proteins were pelleted by centrifugation at 13,000 × g for 15 min at 4 °C. Pellets were washed twice with cold acetone to remove residual TCA, air-dried, and resuspended in SDS sample buffer. Equal volumes of each fraction were analyzed by Western blot. To detect monosialotetrahexosylganglioside (GM1) from each fraction, 1 µl of each of the fractions was loaded on a nitrocellulose membrane, and then wa estern blot was performed with HRP-conjugated cholera toxin subunit B (CT-B) (Sigma).

D4 labeling

The primary retinal microglia cultured on coverslips were washed twice with PBS and fixed 4% paraformaldehyde for 15 min at room temperature. The fixed cells were washed with PBS and permeabilized with PBS containing 0.1% Triton X-100 for 20 min at RT. After washing with PBS, cells were blocked with PBS containing 1% BSA for 45 min at RT. And then incubated with 5 µg/ml His-EGFP-tagged θ toxin domain 4 (His-EGFP-D4) in 1% BSA for 1 hr at RT. The cells were washed and fixed with 4% paraformaldehyde in PBS. Images were acquired using a confocal microscope (LSM980; Zeiss, Germany). His-EGFP-D4 was provided by RIKEN BRC, which is participating in the National Bio-Resources Project of the MEXT, Japan.

Transwell insert chemotaxis assay

Transwells (SPL Life Science, Korea) with an 8 µm pore size were used to measure cell migration. Specifically, 1×10^4 RAW264.7 cells were seeded into the upper chamber, and 500 µL of ARPE19 RPE cell–conditioned medium (RCM) was added to the lower chamber. After 24 h, the cells that remained in the upper chamber were removed with a cotton swab, fixed, and stained with crystal violet (Sigma). Images of the migrated cells were captured using a digital camera connected to an inverted microscope (Olympus IX50, Japan). To quantify cell migration, two complementary approaches were employed. First, migrated cells on the lower surface of the transwell membrane were fixed and stained with crystal violet, and the dye was subsequently eluted using 10% acetic acid. The optical density of the eluate was measured at 595 nm using a microplate reader (Synergy HTX; BioTek, Winooski, VT). In parallel, microscopic images of stained membranes were acquired, and quantification was performed using ImageJ software by measuring the cell-covered area in randomly selected fields.

Immunofluorescence

Retina sections were permeabilized with 0.2% Triton X-100 for 30 min and then blocked in 1% bovine serum albumin (BSA) for 1 h, before being incubated overnight at 4 °C with anti-CD68 (Santa Cruz) and microtubule-associated protein-2 (MAP-2; Abcam, UK) diluted in 1% BSA with 0.2% Triton X-100 in phosphate-buffered saline (PBS). The sections were washed in PBS before being incubated with secondary antibodies (Invitrogen, Carlsbad, CA) for 1 h. The sections were washed in PBS and then mounted with Vectashield medium containing 4',6-diamidino-2-phenylindole (DAPI; Vector Laboratories, Burlingame, CA).

The cells were fixed with 4% paraformaldehyde and then permeabilized with 0.2% Triton X-100 for 10 min. Then, they were washed three times in PBS and blocked with 1% BSA for 1 h, before being incubated with primary antibodies overnight at 4 °C. The cells were then washed and incubated with a fluorescent secondary antibody for 1 h at room temperature. Coverslips were mounted with Vectashield medium containing DAPI and viewed using a confocal microscope (LSM980; Zeiss). Fluorescence images of CD68 and MAP2 staining were analyzed using ImageJ software (NIH, Bethesda, MD), as recommended in the literature[75]. For each sample, fluorescence intensity was measured per field of view in three to five randomly selected regions using identical acquisition settings. The average intensity was calculated after background subtraction.

TUNEL assay

TUNEL assays were conducted using a commercial kit as per the manufacturer's instructions (Promega, Madison, WI). In brief, retina sections were incubated in 1× equilibration buffer for 10 min. Thereafter, the samples were incubated with terminal deoxynucleotidyl transferase for 1 h at 37 °C, blocked with stop/wash buffer, and incubated with a peroxidase antibody for 30 min at room temperature. Coverslips were mounted with Vectashield medium containing DAPI and viewed using a confocal microscope (LSM980, Zeiss). TUNEL-positive cells were quantified based on fluorescence intensity per field of view.

Cell viability assay

Primary neurons were cultured with or without RPE or microglia under 1 G or SMG conditions. After incubation, WST-8 solution (Biomax, Korea) was added to the primary neurons and incubated for 2 h at 37 °C in a CO_2 incubator. The absorbance was measured at 450 nm using an EpochTM microplate reader (BioTek).

Fluorescein isothiocyanate–dextran flux assay

ARPE-19 or primary RPE cells were grown to confluence in transwells with a 0.4 mm polyester membrane (SPL life science) and were maintained in culture for 2–3 weeks in DMEM with 1% FBS. Then, they were incubated under 1G or 10^{-3}G for up to 14 days. The cells were subsequently washed with PBS, and 10 kDa fluorescein isothiocyanate (FITC)–dextran at 1 mg/mL was added to the upper wells for 30 min

(FD10S, Sigma). Next, the medium from the bottom well was used to determine the fluorescence, which was measured using a Synergy HTX plate reader (BioTek) at 485 nm excitation and 520 nm emission.

Depletion of microglia

For microglial depletion, colony stimulating factor 1 receptor (CSF1R) inhibitor, Plexxikon (PLX)5622 (6-Fluoro-*N*-[(5-fluoro-2-methoxypyridin-3-yl) methyl]-5-[(5-methyl-1H-pyrrolo[2,3-*b*] pyridin-3-yl) methyl] pyridin-2-amine; Cayman, Ann Abor, MI) were used. The enucleated eyes were incubated with 0.1 µM PLX5622 or vehicle control (DMSO) for 48 h at 37 °C. Afterward, eyes were incubated under 1G or 10^{-3}G conditions for up to 14 days. PLX5622-mediated microglial depletion was confirmed by analyzing ionized calcium binding adaptor molecule 1 (Iba1) immunoreactivity.

Statistical analysis

The data were plotted using GraphPad Prism 9.5.1. Statistical significance was determined through an unpaired two-tailed Student's *t*-test for pairwise comparisons, and one-way or two-way analysis of variance (ANOVA) for multiple comparisons. Post hoc multiple comparison corrections were performed using the Dunnett method (one-way ANOVA), the Sidak's method (two-way ANOVA). A *p*-value of 0.05 was considered statistically significant. The values are presented as mean ± SD.

Data availability

All data supporting the findings of this study are available within the paper and its Supplementary Information.

Received: 18 November 2024; Accepted: 7 July 2025;
Published online: 01 August 2025

References

1. Mader, T. H. et al. Optic disc edema, globe flattening, choroidal folds, and hyperopic shifts observed in astronauts after long-duration space flight. *Ophthalmology* **118**, 2058–2069 (2011).
2. Michael, A. P. & Marshall-Bowman, K. Spaceflight-induced intracranial hypertension. *Aerosp. Med Hum. Perform.* **86**, 557–562 (2015).
3. Wostyn, P., Mader, T. H., Gibson, C. R. & Nedergaard, M. Does long-duration exposure to microgravity lead to dysregulation of the brain and ocular glymphatic systems?. *Eye Brain.* **14**, 49–58 (2022).
4. Lee, A. G. et al. Spaceflight associated neuro-ocular syndrome (SANS) and the neuro-ophthalmologic effects of microgravity: a review and an update. *NPJ Microgravity* **6**, 7 (2020).
5. Crucian, B. E. et al. Plasma cytokine concentrations indicate that in vivo hormonal regulation of immunity is altered during long-duration spaceflight. *J. Interferon Cytokine Res.* **34**, 778–786 (2014).
6. Zanello, S. B., Theriot, C. A., Ponce, C. M. P. & Chevez-Barrios, P. Spaceflight effects and molecular responses in the mouse eye: preliminary observations after shuttle mission STS-133. *Gravit. Space Res.* **1**, 29–46 (2013).
7. Norris, G. T. & Kipnis, J. Immune cells and CNS physiology: Microglia and beyond. *J. Exp. Med.* **216**, 60–70 (2019).
8. Silverman, S. M. & Wong, W. T. Microglia in the Retina: Roles in Development, Maturity, and Disease. *Annu Rev. Vis. Sci.* **4**, 45–77 (2018).
9. Li, L., Eter, N. & Heiduschka, P. The microglia in healthy and diseased retina. *Exp. Eye Res.* **136**, 116–130 (2015).
10. Cherry, J. D., Olschowka, J. A. & O'Banion, M. K. Neuroinflammation and M2 microglia: the good, the bad, and the inflamed. *J. Neuroinflamm.* **11**, 98 (2014).
11. Block, M. L., Zecca, L. & Hong, J. S. Microglia-mediated neurotoxicity: uncovering the molecular mechanisms. *Nat. Rev. Neurosci.* **8**, 57–69 (2007).
12. Zhao, L. et al. Microglial phagocytosis of living photoreceptors contributes to inherited retinal degeneration. *EMBO Mol. Med.* **7**, 1179–1197 (2015).
13. Lin, T. et al. Treatment with Minocycline suppresses microglia activation and reverses neural stem cells loss after simulated microgravity. *Biomed. Res. Int.* **2020**, 7348745 (2020).
14. Chelyshev, Y. A. et al. Characterization of spinal cord glial cells in a model of hindlimb unloading in mice. *Neuroscience* **280**, 328–339 (2014).
15. Paulsen, K. et al. Regulation of ICAM-1 in cells of the monocyte/macrophage system in microgravity. *Biomed. Res. Int.* **2015**, 538786 (2015).
16. Grassi, S. et al. Lipid rafts and neurodegeneration: structural and functional roles in physiologic aging and neurodegenerative diseases. *J. Lipid Res.* **61**, 636–654 (2020).
17. Miller, Y. I., Navia-Pelaez, J. M., Corr, M. & Yaksh, T. L. Lipid rafts in glial cells: role in neuroinflammation and pain processing. *J. Lipid Res.* **61**, 655–666 (2020).
18. Varshney, P., Yadav, V. & Saini, N. Lipid rafts in immune signalling: current progress and future perspective. *Immunology* **149**, 13–24 (2016).
19. Ruysschaert, J. M. & Lonez, C. Role of lipid microdomains in TLR-mediated signalling. *Biochim. Biophys. Acta* **1848**, 1860–1867 (2015).
20. Blouin, C. M. & Lamaze, C. Interferon gamma receptor: the beginning of the journey. *Front. Immunol.* **4**, 267 (2013).
21. Woo, J. H., Park, S. J., Park, S. M., Joe, E. H. & Jou, I. Interleukin-6 signaling requires EHD1-mediated alteration of membrane rafts. *FEBS J.* **289**, 5914–5932 (2022).
22. Legler, D. F., Micheau, O., Doucey, M. A., Tschopp, J. & Bron, C. Recruitment of TNF receptor 1 to lipid rafts is essential for TNFalpha-mediated NF-kappaB activation. *Immunity* **18**, 655–664 (2003).
23. Brown, A. J. & Jessup, W. Oxysterols: Sources, cellular storage and metabolism, and new insights into their roles in cholesterol homeostasis. *Mol. Asp. Med.* **30**, 111–122 (2009).
24. Spann, N. J. & Glass, C. K. Sterols and oxysterols in immune cell function. *Nat. Immunol.* **14**, 893–900 (2013).
25. Olkkonen, V. M., Beaslas, O. & Nissila, E. Oxysterols and their cellular effectors. *Biomolecules* **2**, 76–103 (2012).
26. Zhang, X. et al. Oxysterols and retinal degeneration. *Br. J. Pharmacol.* **178**, 3205–3219 (2021).
27. Lee, J. H., Han, J. H., Woo, J. H. & Jou, I. 25-Hydroxycholesterol suppress IFN-gamma-induced inflammation in microglia by disrupting lipid raft formation and caveolin-mediated signaling endosomes. *Free Radic. Biol. Med.* **179**, 252–265 (2022).
28. Dang, E. V., McDonald, J. G., Russell, D. W. & Cyster, J. G. Oxysterol restraint of cholesterol synthesis prevents AIM2 inflammasome activation. *Cell* **171**, 1057–71.e11 (2017).
29. Reboldi, A. et al. Inflammation. 25-Hydroxycholesterol suppresses interleukin-1-driven inflammation downstream of type I interferon. *Science* **345**, 679–684 (2014).
30. Cyster, J. G., Dang, E. V., Reboldi, A. & Yi, T. 25-Hydroxycholesterols in innate and adaptive immunity. *Nat. Rev. Immunol.* **14**, 731–743 (2014).
31. Massey, J. B. & Pownall, H. J. The polar nature of 7-ketocholesterol determines its location within membrane domains and the kinetics of membrane microsolubilization by apolipoprotein A-I. *Biochemistry* **44**, 10423–10433 (2005).
32. Wang, S. et al. Cholesterol 25-Hydroxylase inhibits SARS-CoV-2 and other coronaviruses by depleting membrane cholesterol. *EMBO J.* **39**, e106057 (2020).
33. Mishra, S. & Joshi, P. G. Lipid raft heterogeneity: an enigma. *J. Neurochem.* **103**, 135–142 (2007).
34. Li, S. et al. Structural damage to the rat eye following long-term simulated weightlessness. *Exp. Eye Res.* **223**, 109200 (2022).

35. Jurga, A. M., Paleczna, M. & Kuter, K. Z. Overview of general and discriminating markers of differential microglia phenotypes. *Front Cell Neurosci.* **14**, 198 (2020).
36. O'Leary, F. & Campbell, M. The blood-retina barrier in health and disease. *FEBS J.* **290**, 878–891 (2023).
37. Obert, E. et al. Targeting the tight junction protein, zonula occludens-1, with the connexin43 mimetic peptide, alphaCT1, reduces VEGF-dependent RPE pathophysiology. *J. Mol. Med.* **95**, 535–552 (2017).
38. Ablonczy, Z. & Crosson, C. E. VEGF modulation of retinal pigment epithelium resistance. *Exp. Eye Res.* **85**, 762–771 (2007).
39. Bandyopadhyay, M. & Rohrer, B. Matrix metalloproteinase activity creates pro-angiogenic environment in primary human retinal pigment epithelial cells exposed to complement. *Invest Ophthalmol. Vis. Sci.* **53**, 1953–1961 (2012).
40. Laurie S. S. et al. Risk of spaceflight associated neuro-ocular syndrome (SANS) 2022 [Available from: https://humanresearchroadmap.nasa.gov/evidence/reports/SANS%20EB%202022%20FINAL_8-15-22.pdf.
41. Traon AP-L., Petersen L., Claudia Stern Y. Y., Eulenburg P. Z. ESA SciSpacE White Papers, #12: Human Physiology 2021 [Available from: https://esamultimedia.esa.int/docs/HRE/12_HumanResearch_HumanPhysiology.pdf.
42. O'Koren, E. G., et al. Microglial function is distinct in different anatomical locations during retinal homeostasis and degeneration. *Immunity* **50**, 723–37.e7 (2019).
43. Karg, M. M. et al. Microglia preserve visual function loss in the aging retina by supporting retinal pigment epithelial health. *Immun. Ageing* **20**, 53 (2023).
44. Wieghofer, P. et al. Mapping the origin and fate of myeloid cells in distinct compartments of the eye by single-cell profiling. *EMBO J.* **40**, e105123 (2021).
45. Benhar, I., Reemst, K., Kalchenko, V. & Schwartz, M. The retinal pigment epithelium as a gateway for monocyte trafficking into the eye. *EMBO J.* **35**, 1219–1235 (2016).
46. Elmore, M. R. et al. Colony-stimulating factor 1 receptor signaling is necessary for microglia viability, unmasking a microglia progenitor cell in the adult brain. *Neuron* **82**, 380–397 (2014).
47. Lei, F., et al. CSF1R inhibition by a small-molecule inhibitor is not microglia specific; affecting hematopoiesis and the function of macrophages. *Proc. Natl. Acad. Sci. USA.* **117**, 23336–23338 (2020).
48. Yu, C. et al. Microglia at sites of atrophy restrict the progression of retinal degeneration via galectin-3 and Trem2. *J. Exp. Med*. **221**, e20231011 (2024).
49. Cliver, R. N. et al. Antioxidants derived from natural products reduce radiative damage in cultured retinal Glia to prevent oxidative stress. *Neurogl. [Internet].* **3**, 84–98 (2022).
50. Uva, B. M. et al. Clinorotation-induced weightlessness influences the cytoskeleton of glial cells in culture. *Brain Res.* **934**, 132–139 (2002).
51. Grigoryan, E. N. et al. Signs of Müller cell gliotic response found in the retina of newts exposed to real and simulated microgravity. *Adv. Space Res.* **49**, 1465–1471 (2012).
52. Hu, X. et al. Interplay between Muller cells and microglia aggravates retinal inflammatory response in experimental glaucoma. *J. Neuroinflamm.* **18**, 303 (2021).
53. Di Pierdomenico, J. et al. Coordinated intervention of microglial and muller cells in light-induced retinal degeneration. *Invest Ophthalmol. Vis. Sci.* **61**, 47 (2020).
54. Wang, M. & Wong, W. T. Microglia-Muller cell interactions in the retina. *Adv. Exp. Med. Biol.* **801**, 333–338 (2014).
55. Kugler, E. C., Greenwood, J. & MacDonald, R. B. The "Neuro-Glial-Vascular" Unit: The role of Glia in neurovascular unit formation and dysfunction. *Front Cell Dev. Biol.* **9**, 732820 (2021).
56. Reichenbach, A. & Bringmann, A. New functions of Muller cells. *Glia* **61**, 651–678 (2013).
57. Carpi-Santos, R., de Melo Reis, R. A., Gomes, F. C. A. & Calaza, K. C. Contribution of Muller cells in the diabetic retinopathy development: focus on oxidative stress and inflammation. *Antioxidants* **11**, 617 (2022).
58. Leoni, V. & Caccia, C. Oxysterols as biomarkers in neurodegenerative diseases. *Chem. Phys. lipids* **164**, 515–524 (2011).
59. Fliesler, S. J. & Bretillon, L. The ins and outs of cholesterol in the vertebrate retina. *J. Lipid Res.* **51**, 3399–3413 (2010).
60. Rodriguez, I. R. & Larrayoz, I. M. Cholesterol oxidation in the retina: implications of 7KCh formation in chronic inflammation and age-related macular degeneration. *J. Lipid Res.* **51**, 2847–2862 (2010).
61. Rodriguez, I. R., Clark, M. E., Lee, J. W. & Curcio, C. A. 7-ketocholesterol accumulates in ocular tissues as a consequence of aging and is present in high levels in drusen. *Exp. Eye Res.* **128**, 151–155 (2014).
62. Biswas, L., Farhan, F., Reilly, J., Bartholomew, C. & Shu, X. TSPO ligands promote cholesterol efflux and suppress oxidative stress and inflammation in choroidal endothelial cells. *Int. J. Mol. Sci.* **19**, 3740 (2018).
63. Biswas, L., Zhou, X., Dhillon, B., Graham, A. & Shu, X. Retinal pigment epithelium cholesterol efflux mediated by the 18 kDa translocator protein, TSPO, a potential target for treating age-related macular degeneration. *Hum. Mol. Genet.* **26**, 4327–4339 (2017).
64. Joffre, C. et al. Oxysterols induced inflammation and oxidation in primary porcine retinal pigment epithelial cells. *Curr. Eye Res.* **32**, 271–280 (2007).
65. Dugas, B. et al. Effects of oxysterols on cell viability, inflammatory cytokines, VEGF, and reactive oxygen species production on human retinal cells: cytoprotective effects and prevention of VEGF secretion by resveratrol. *Eur. J. Nutr.* **49**, 435–446 (2010).
66. Rodriguez, I. R., Alam, S. & Lee, J. W. Cytotoxicity of oxidized low-density lipoprotein in cultured RPE cells is dependent on the formation of 7-ketocholesterol. *Invest Ophthalmol. Vis. Sci.* **45**, 2830–2837 (2004).
67. Olivier, E. et al. P2X7-pannexin-1 and amyloid beta-induced oxysterol input in human retinal cell: Role in age-related macular degeneration?. *Biochimie* **127**, 70–78 (2016).
68. Odnoshivkina, U. G., Kuznetsova, E. A. & Petrov, A. M. 25-Hydroxycholesterol as a signaling molecule of the nervous system. *Biochemistry.* **87**, 524–537 (2022).
69. Gao, C., Jiang, J., Tan, Y. & Chen, S. Microglia in neurodegenerative diseases: mechanism and potential therapeutic targets. *Signal Transduct. Target Ther.* **8**, 359 (2023).
70. Zhang, G., Wang, Z., Hu, H., Zhao, M. & Sun, L. Microglia in Alzheimer's disease: a target for therapeutic intervention. *Front Cell Neurosci.* **15**, 749587 (2021).
71. Del Amo, E. M. et al. Pharmacokinetic aspects of retinal drug delivery. *Prog. Retin Eye Res.* **57**, 134–185 (2017).
72. Fernandes, A. et al. Short-term free-floating slice cultures from the adult human brain. *J. Vis. Exp* **153**, e59845 (2019).
73. Otsuka, T. et al. Simulated microgravity culture enhances the neuroprotective effects of human cranial bone-derived mesenchymal stem cells in traumatic brain injury. *Stem Cells Dev.* **27**, 1287–1297 (2018).
74. Furukawa, T. et al. Simulated microgravity attenuates myogenic differentiation via epigenetic regulations. *NPJ Microgravity* **4**, 11 (2018).
75. Rueden, C. T. et al. ImageJ2: ImageJ for the next generation of scientific image data. *BMC Bioinforma.* **18**, 529 (2017).

Acknowledgements

This research was supported by the National Research Foundation of Korea (RS-2018-NR031065 and RS-2023-NR076534), by the Korea Medical Device Development Fund grant funded by the Korea government (the Ministry of Science and ICT, the Ministry of Trade, Industry and Energy, the Ministry of Health & Welfare, the Ministry of Food and Drug Safety) (Project Number: RS-2023-00242778).

Author contributions

J.H.L. and D.Y.K. contributed to the conception and experimental design of the study. J.H.L. performed the biological experiments, analyzed the data, and prepared the figures and tables. J.H.L. and D.Y.K. wrote and edited the manuscript. D.Y.K. provided the overall project leadership. All the authors have read and approved the final manuscript.

Competing interests

The authors declare no competing interests.

Additional information

Supplementary information The online version contains supplementary material available at https://doi.org/10.1038/s41526-025-00507-7.

Correspondence and requests for materials should be addressed to Dae Yu Kim.